Emergence and spread of feline infectious peritonitis due to a highly pathogenic canine/feline recombinant coronavirus

Charalampos Attipa[1,2◇*], Amanda S Warr[2◇*], Demetris Epaminondas[3], Marie O'Shea[2], Sarah Fletcher[2], Alexandra Malbon[2,3], Maria Lyraki[4], Rachael Hammond[1], Alexandros Hardas[5], Antria Zanti[6], Stavroula Loukaidou[6], Michaela Gentil[7], Danielle Gunne-Moore[1], Stella Mazeri[2], Christine Tait-Burkard[2*]

[1]Royal (Dick) School of Veterinary Studies, University of Edinburgh, Easter Bush, Midlothian, United Kingdom.

[2]The Roslin Institute, Royal (Dick) School of Veterinary Studies, University of Edinburgh, Easter Bush, Midlothian, United Kingdom.

[3]Veterinary Services, Ministry of Agriculture, Natural Resources and Environment, Cyprus.

[4]Plakentia Veterinary Clinic, Athens, Greece.

[5]Department of Pathobiology and Population Sciences, Royal Veterinary College, Hatfield, Hertfordshire.

[6]Vet Dia Gnosis Ltd, Limassol, Cyprus.

[7]Laboklin GmbH and Co KG, Bad Kissingen, Germany.

◇Contributed equally to this work. CA was responsible for epidemiology, pathology and sample/outbreak data collection. AW performed sequencing and data analysis thereof. Both are equally important but the latter couldn't have happened without the first.

*Corresponding authors

Email: charalampos.attipa@ed.ac.uk

Email: Amanda.warr@roslin.ed.ac.uk

Email: christine.burkard@roslin.ed.ac.uk

Abstract

Cross-species transmission of coronaviruses (CoVs) poses a serious threat to both animal and human health[1-3]. Whilst the large RNA genome of CoVs shows relatively low mutation rates, recombination within genera is frequently observed and demonstrated[4-7]. Companion animals are often overlooked in the transmission cycle of viral diseases; however, the close relationship of feline (FCoV) and canine CoV (CCoV) to human hCoV-229E[5,8], as well as their susceptibility to SARS-CoV-2[9] highlight their importance in potential transmission cycles. Whilst recombination between CCoV and FCoV of a large fragment spanning orf1b to M has been previously described[5,10], here we report the emergence of a novel, highly pathogenic FCoV-CCoV recombinant responsible for a rapidly spreading outbreak of feline infectious peritonitis (FIP), originating in Cyprus[11]. The recombination, spanning spike, shows 97% sequence identity to the pantropic canine coronavirus CB/05. Infection is spreading fast and infecting cats of all ages. Development of FIP appears rapid and likely non-reliant on biotype switch[12]. High sequence identity of isolates from cats in different districts of the island is strongly supportive of direct transmission. A deletion and several amino acid changes in spike, particularly the receptor binding domain, compared to other FCoV-2s, indicate changes to receptor binding and likely cell tropism.

Main

Following two epidemics, SARS-CoV 2002-4 and MERS-CoV 2012-ongoing, and a pandemic of previously unseen proportions, SARS-CoV-2 2019 onwards, coronaviruses no longer need lengthy introductions of importance and scale. They are not only present in the human population, they are also in wildlife[13-15], companion animals[16-19] and livestock[13,20,21], and in all species these viruses have major impacts. The innate ability of coronaviruses to recombine with other coronaviruses continues to fuel their species-switching ability. It is therefore not surprising that both human and animal coronaviruses are linked in complex transmission and evolution cycles[3,14,19,22].

FCoV is found across the globe. The virus exists in two biotypes with the main biotype, feline enteric coronavirus (FECV), showing low virulence and clinical signs are typically limited to mild enteritis. The second biotype of FCoV, proposed to originate each time from a mutation in an FECV-infected cat (reviewed in [23]), is known as feline infectious peritonitis virus (FIPV). FIPV causes feline infectious peritonitis (FIP), which is a fatal disease if left untreated. Clinical signs include an abdomen swollen due to peritoneal fluid, fever, weight loss lethargy, anorexia, dyspnoea, ocular abnormalities and neurological signs[8,16,24,25]. Mutations in the spike gene or the accessory genes 3abc and of 7ab of FCoV[8,16,23,26] are thought to result in changes to the virus's tropism from cells in the enteric tract to macrophages, resulting in the different disease

2

65   presentation seen with the two biotypes. This change in primary tropism also impacts the virus's

66   ability to transmit from cat to cat, with the main transmission pathway of FECV being faecal-oral

67   and FIPV typically having relatively poor transmission potential. Antivirals, including remdesivir

68   and GS-441524 have recently been successfully used to treat cats with FIP[27].

69   FCoV and CCoV both belong to the *Alphacoronavirus 1* species alongside the porcine transmissible

70   gastroenteritis virus (TGEV) and, probably, the never fully sequenced rabbit enteric

71   coronavirus[28,29]. Both FCoV and CCoV have evolved two different serotypes through complex

72   recombination events between the two viruses with a suspected gradual evolution from CCoV-II

73   to TGEV and the later spike deletion to porcine respiratory coronavirus (PRCV)[23,30]. Whilst

74   recombination events between CCoV and FCoV have significantly contributed to the serotype

75   evolution and have been frequently described, so far, none of them lead to enhanced

76   transmissibility of FIP beyond closest contact[10,23,31,32]. Similarly, recombination events have been

77   reported between CCoV and TGEV[33], the latter has been found to recombine with the

78   pedacoronavirus (alphacoronavirus genus) porcine epidemic diarrhoea virus[6]. These

79   observations are particularly important in view of the *Alphacoronavirus 1*-related human

80   infections recently observed[19,22].

81   Earlier this year, we alerted the veterinary field to an outbreak of FIP in Cyprus, where there had

82   been a concerning increase in cases[11]. Cases were recorded as FIP only if they had compatible

83   clinicopathological signs and a positive RT-qPCR for FCoV in one of the following samples;

84   peritoneal fluid, pleural fluid, cerebrospinal fluid, fine needle aspiration biopsies, or tissue

85   biopsies from granulomatous lesions. In comparison, in 2021 and 2022, there were three and four

86   RT-qPCR confirmed FIP cases recorded in Cyprus, respectively, to date in 2023 (January-August),

87   165 cases have been confirmed. This represents more than a 40-fold increase. The outbreak

88   emerged in January 2023 in Nicosia, the capital of Cyprus. An increase in cases was first observed

89   in January 2023 and by February Nicosia recorded the peak number of cases in any district

90   (Figure 1A & B). The next highest number of cases was observed in Famagousta, which peaked in

91   March, and by then the outbreak had spread to all districts of the Republic of Cyprus.

92   (Supplementary Tables 1-5). In June and July there was a decline in RT-qPCR confirmed cases,

93   which coincided with a large media awareness campaign to alert veterinarians to the spread of

94   FIP[11]. This fall in RT-qPCR confirmed cases is likely due to most veterinarians diagnosing cases

95   based on clinicopathological findings without performing PCR testing due to the additional

96   financial cost. On August 3rd, the Republic of Cyprus minister's cabinet approved the use of the

97   stocked human coronavirus medications to be used for cats with FIP. In order for veterinarians

98   to have access to this medication, amongst others, a PCR confirmation was required, reflecting

99   the increased cases seen during August 2023. In order for veterinarians to have access to this

100 medication a PCR confirmation was required, reflecting the increased cases seen during August

101 2023 (Figure 1A & B). The number of unreported cases in Cyprus is very high, not least due to the

102 high number of feral cats. Estimates from the Pancyprian Veterinary Association indicate around

103 8,000 deaths due to FIP up to mid-July 2023. Furthermore, in October 2023, a first imported case

104 of FIP was confirmed in the UK.

105
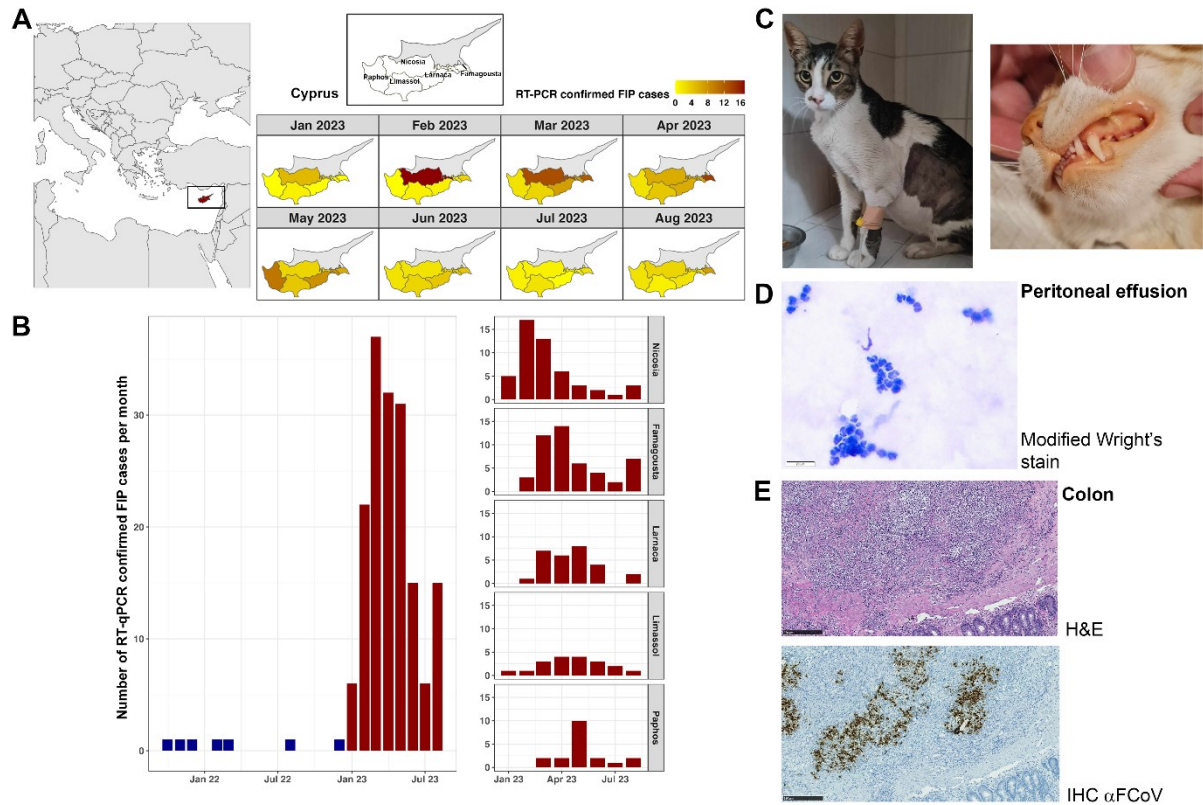
Figure 1: Epidemiology and Pathology of the FIP outbreak in Cyprus, 2023. A) Distribution of RT-PCR confirmed positive FIP cases across Cyprus. First image locates Cyprus within the Easter Mediterranean. Darker colors indicate higher numbers of confirmed cases over time within each district. **B)** RT-PCR confirmed case rates resolved by time and province. **C)** Clinical presentation of cats with FIP due to FCoV-23. Left; cat with the effusive form of FIP showing abdominal distention due to peritoneal effusion, an unkept coat, low body condition score, and poor muscle condition. Right; cat presenting with jaundice evidenced by yellow/orange discoloration of the mucous membranes and mucocutaneous junctions. Images courtesy of Eva Georgiadi. **D)** Photomicrograph of fluid smear from a peritoneal effusion from a cat with confirmed FIP due to FCoV-23 infection. Non-degenerative neutrophils are present on a protein rich background shown using a Modified Wright's stain. Scale bar represents 20μm. E) Photomicrographs showing a section of colonic mucosa and submucosa from a cat with confirmed FIP due to FCoV-23 infection. Top; H&E-stained histology section shows coalescing infiltration of predominantly the submucosa by aggregates of primarily neutrophils and macrophages surrounded by fewer lymphocytes and plasma cells. The muscularis mucosae is disrupted by the inflammation. Bottom; Immunohistochemistry staining against FCoV in a histology section mirroring the above. Extensive positive FCoV cytoplasmic staining for cells at the center of each aggregate/pyogranuloma in cells with macrophage-like morphology. Scale bar represents 200μm.

119 The most common clinical form of FIP was effusive (69.7%; Figure 1C), followed by neurological

120 FIP (27.9%) and the non-effusive form (2.4%) (Supplementary table 4). Where peritoneal fluid

121 was assessed by cytology, non-degenerative neutrophils admixed with macrophages and small

122 lymphocytes were seen in a protein rich background (Figure 1D). Five cases were assessed by

123 histopathology, including intestinal mass (n=1), lymph node (n=2), and kidney (n=2). All showed

4

124   similar histological features, with multifocal to coalescing, pyogranulomatous to necrotising and

125   lymphoplasmacytic inflammation (Figure 1E). The angiocentric nature can be seen in some areas,

126   whilst in others there is total effacement of the tissue. Immunohistology for FCoV antigen

127   demonstrated a heavy viral load within intralesional macrophages (Figure 1E).

128   RNA samples were obtained from 91 confirmed FIP cases between 2021 and 2023, representing

129   a mixture of geographic origin, sex, and clinical presentation (Supplementary Tables 6-11). They

130   were sequenced using cDNA/PCR-amplification-based Nanopore sequencing to better

131   understand the outbreak and to determine if cat-to-cat transmission of FIPV is occurring.

132   Additional samples were submitted from two cats presenting with FIP following recent import

133   from Cyprus to the UK. Initial focus laid on amplification of the spike, which was successful in 43

134   of the Cypriot samples and in the two imported UK cat samples. The other samples were degraded

135   or contained too few viral copies. None of the seven samples from before 2023 amplified

136   (Supplementary Tables 12-17). Other regions of the genome were amplified in several

137   individuals; however, none of the cats had the entire genome amplified due to intentional

138   conservation of limited samples until a working primer scheme is designed for the entire genome.

139   The sequenced spike region of the FCoV samples produced three distinct versions of the spike

140   sequence. BLAST was used to identify close relatives of these spike sequences. The first is a spike

141   sequence most closely related to an FCoVI (genbank ID MT444152.1) with 79% similarity, which

142   occurred in one Cypriot and one UK-import sample, and the other two are almost entirely CCoVII

143   spike sequence, flanked by FCoVI sequence. The CCoVII sequence is most closely related to the

144   NA/09 strain (GB JF682842), a hypervirulent pantropic canine coronavirus (pCCoV)[34], at 97%

145   sequence identity. The spike sequence is also closely related to other pCCoV spike sequences with

146   only partial spike sequences available (Figure 2, Supplementary Figure 1). Two of the samples,

147   one Cypriot and one UK-import case, showed high similarity with FIPV-1 spikes. However, all

148   other samples, including one UK-import case align with a pCCoV spike. This is likely a defining

149   feature of the virus circulating in the outbreak in Cyprus. There are two versions of this spike

150   gene, one of which has a deletion of approximately 630bp near the beginning of the spike

151   sequence in the N terminal domain, and this deletion version is present in the majority, 35/43 of

152   the pCCoV spikes sequenced.

153   Regions of POL1ab and ORF3c/E/M were amplified in several of the cats in addition to the spike

154   genes. These sequences and the spike sequences were individually aligned to the CCoVII, FCoVI

155   and FCoVII whole genome sequences available on NCBI. Figure 2 shows maximum likelihood

156   trees all three different regions (also Supplementary Figures 2-4). While the POL1ab and

157   ORF3c/E/M amplicons all cluster with FCoVI, the spike sequences cluster with CCoVII, most

158   closely with the pantropic strains NA/09 and CB/05. The spike amplicon from one UK-import cat

159   clusters among the spike sequences from the outbreak in Cyprus.
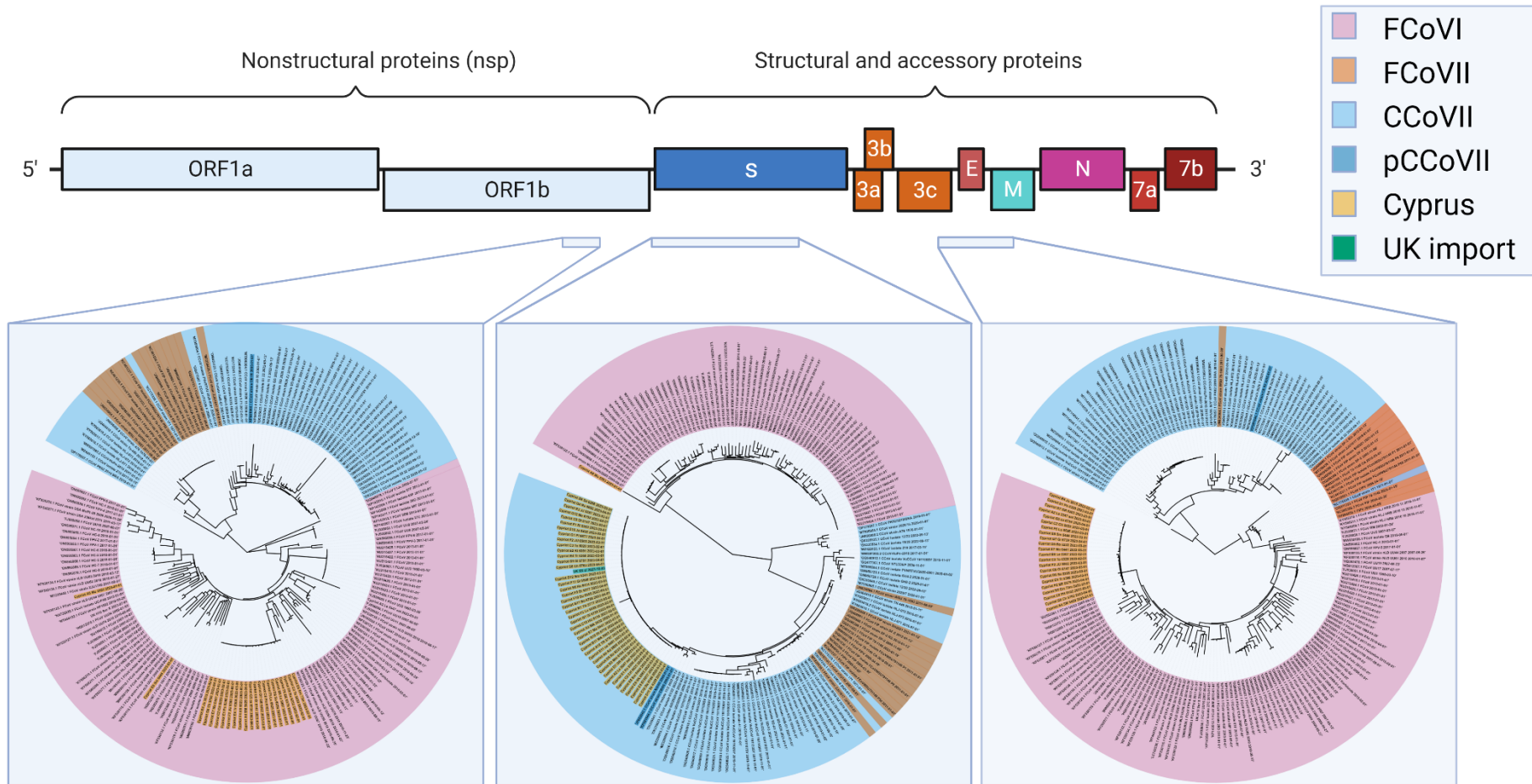
Figure 2: Genomic sequence analysis of Cypriot/UK-import FCoV cases. Sequences from three different genomic regions: Orf1b, spike, and Orf3c/E/M, as indicated by the regions marked on the overview of the genome, were obtained through Nanopore sequencing from 22, 45, and 22, Cypriot and UK-import samples, respectively. Following initial BLAST analysis, maximum likelihood trees were generated including other FCoV and CCoV strains to assess genetic similarity of each region. CCoVII genomes are highlighted in light blue with pCCoVII genomes within this region displayed in a darker blue. FCoVI genomes are highlighted in pink and FCoVII genomes in orange. Samples from Cyprus (Yellow) and one UK-imported Cypriot cat (Green) can be seen clustered with FCoVI sequences in the Orf1b and Orf3c/E/M regions. The spike gene, however, clusters with CCoVII, most closely with pCCoVII. Different numbers of sequences are present in each tree due to missing sequence or poor sequence quality and/or alignments in genomes downloaded from NCBI, and due to not all regions being sequenced in all individuals from our samples. The figure was created with Biorender.
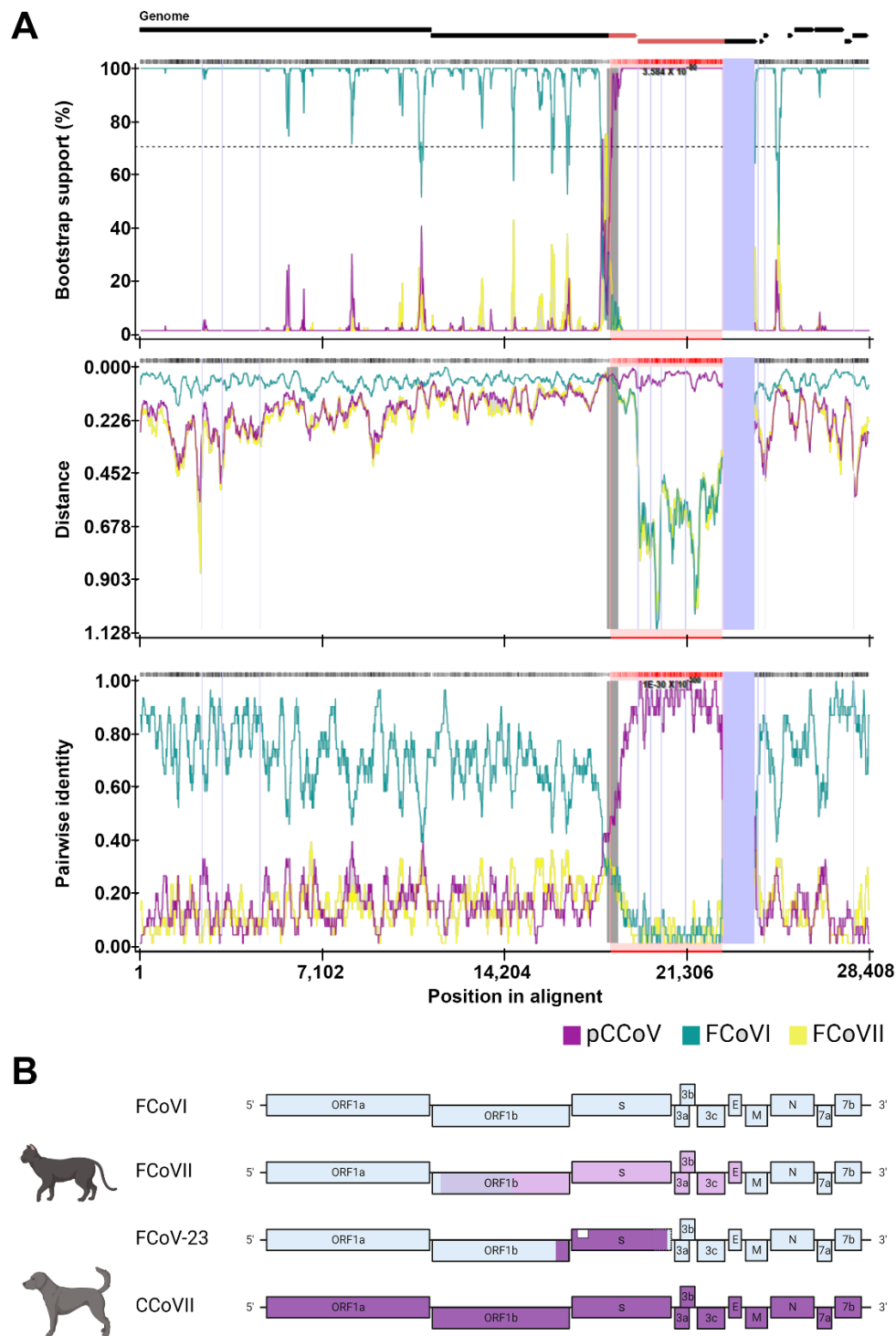
Figure 3: Recombination analysis. A) Visualizations of a recombination analysis carried out on the assembled FCoV-23 genome and representative genomes of FCoVI (green), FCoVII (yellow) and pCCoV (purple). An annotated sequence can be found in Supplementary File 1 and will be deposited to Genbank prior to publication. The blue panel shows the gap in the assembled genome, and the grey panel shows the likely recombination break region, with an orange vertical line showing the likely break point. The first panel shows the results of the Bootscan analysis, the second panel shows the sequence distance, and the third panel shows the RDP pairwise identity analysis. All three panels show good support for the recombination between FCoVI and pCCoV. These results are further supported by high statistical likelihood of recombination shown in Supplementary Table 19. **B)** Schematic representation of major recombinations observed in FCoV and CCoV. A common ancestral origin virus is thought to have given rise to the original FCoVI and CCoVI types with further evolution in CCoVs yielding CCoVII and CCoVI/II serotypes. FCoVs are thought to have recombined with CCoVII to form FCoVII. FCoVII/CCoVII recombinations have shown to have different recombination points as highlighted by the different colorations (reviewed in [23]). The Cypriot FCoV strain, termed FCoV-23, is a recombinant between an FCoVI strain and a spike recombination with a pantropic CCoVII, pCCoV. Furthermore, a deletion variant is observed in a majority of sequenced cases (white box).

8

181 A representative genome of FCoV-23 was assembled from amplicons amplified from multiple
182 Cypriot samples (Supplementary File 1), a single gap of 1,221bp remains in this assembly at the
183 second recombination breakpoint. Supplementary Figure 5 shows a neighbour joining tree for
184 the assembled coronavirus along with other members of *Alphacoronavirus 1* and a distantly
185 related Canine Respiratory Coronavirus as an outgroup. The assembled genome clusters with
186 representatives of FCoVI, similar to the clustering of the amplicons outside of the spike region.

187 A recombination analysis was carried out comparing the FCoV-23 genome with FCoVI, FCoVII and
188 CCoVII strain CB/05, since NA/09 is not available as a complete genome. Figure 3A shows
189 visualisations of the Bootscan[35] analysis, the RDP5[36] analysis and the pairwise distances between
190 the sequences. Significant p-values supporting the recombination were reported by multiple
191 methods as listed in Supplementary Table 19. The MaxChi[37] breakpoint matrix is available in
192 Supplementary Figure 6. Despite the second breakpoint being missing from the analysis due to
193 the remaining gap in the genome, the recombination is very clear and includes a small region of
194 the POL1b gene and the majority of the spike gene, but none of the genes to the 3` end of spike.
195 Some reads, while not sufficiently high coverage to create a consensus for this gap region, suggest
196 that the recombination break point occurs within the spike gene, close to the 3` end
197 (Supplementary Figure 7). Figure 3B shows the historical break point between FCoVI and CCoVII
198 that created FCoVII alongside the recombination identified here.

199 The main determinant in disease development and transmission of FCoV-23 appears to be the
200 spike recombination. One of the main suggested determinants of biotype changes, the furin
201 cleavage site (FCS) at the S1/S2 interface[23,26] is absent in FCoVIIs and also FCoV-23. An interesting
202 observation, however, is that the majority of samples show a deletion in domain 0, strongly
203 resembling the deletion observed in TGEV and porcine respiratory coronavirus (PRCV) (Figure
204 4A). In other coronaviruses, including TGEV[38] and CCoV-HuPn-2018[39], domain 0 was shown to
205 bind sialosides. Modelling the structure of spike against the closely related, experimentally
206 confirmed CCOV-HuPn-2018 spike[39] shows a much more compact confirmation for the domain 0
207 deletion spike and similarity to a structural prediction based on a "swung-out" or a "proximal"
208 confirmation template (Figure 4B, Supplementary Figure 8). A number of amino acid changes
209 were observed between "classical" FECV-2 and FIPV-2 spikes. In particular domains A and B, the
210 receptor binding domain (RBD) show a number of class changing amino acid changes distinct
211 from FCoV-2 spikes (Figure 4A). Modelling the RBD changes against the structure highlights
212 changes at positions 546 and 595, as well as 556, 603, and 636 as being potentially strongly
213 influential to receptor binding properties (Figure 4C).

214 Previously indicated key proteins for biotype switch spike, Orf3abc and 7b were compared to the
215 recently published computational analysis of mutations observed in FECV versus FIPV by Zehr *et*

216   *al.*[26]. Unfortunately, the suggested key determinant of FIPV in the FCoV-2 spike, position 1404, is

217   not yet resolved in FCoV-23. Other positions in spike show new mutations or are suggestive of

218   FIPV (Supplementary Table 20). Whilst a new mutation each was identified in Orf3a and b, no

219   specific indications of pathogenesis could be determined (Supplementary Table 21). Similarly, in

220   Orf7b, two new mutations but no indication of pathogenesis could be identified (Supplementary

221   Table 22).
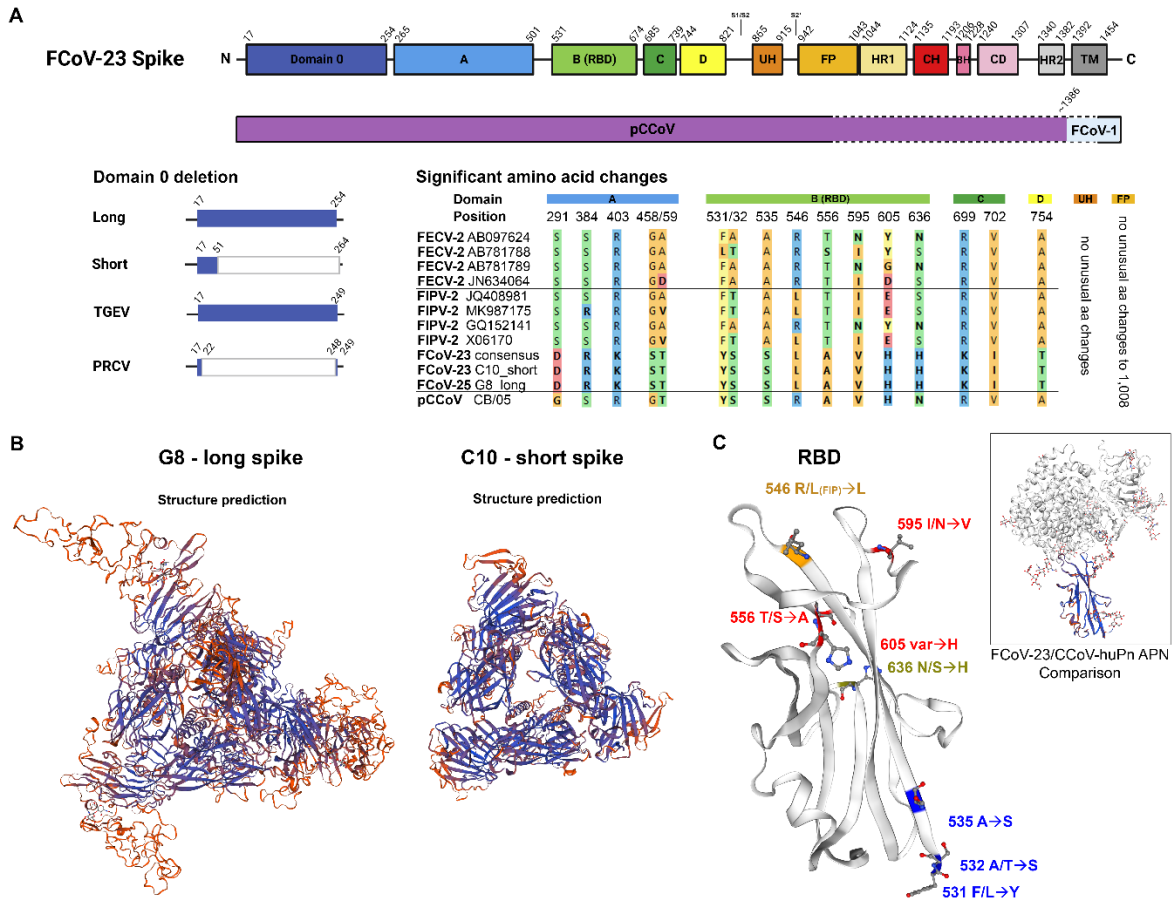
222

223 **Figure 4: Protein sequence and structural analysis of FCoV-23 Spike. A)** Analysis of the different domains of FCoV-23 spike.

224 Sequencing depth in the regions highlighted with a dashed border are not sufficient to call individual bases with enough certainty to

225 perform sequence analysis. Therefore, these regions have been excluded here. Domain 0 in its full-length version shows high similarity

226 to CB/05 pCCoV; however most prominent is the large deletion from aa51-264 strongly resembling the deletion previously observed

227 between the TGEV and PRCV spike. Multi-sequence alignment was performed against four confirmed FECV-2 and four confirmed

228 FIPV-2 mirroring sequences used for computational analysis by Zehr *et al.*[26]. Highlighted are amino acid changes with significant

229 change against FCoVIIs and also position 546, where a Leucin is more predominant in FIPV rather than FECV sequences. Colors are

230 following the RasMol amino acid color scheme. **B)** Structural modelling of the "full-length" or long spike version, represented by

231 sample G8, and the "domain 0 deletion" or short version, represented by sample C10. Samples were modelled against the CCoV-HuPN-

232 2018, experimentally determined spike in the swung out confirmation 7usa.1.A[39]. The proximal confirmation and comparisons may

233 be found in Supplementary Figure 8. Colors indicate confidence with blue highlighting strong and red highlighting weak confidence.

234 **C)** Modelling or amino acid changes on a structural prediction of the FCoV-23 RBD against CCoV-HuPN-2018 7u8I.1.B. Significant

235 amino acid changes as identified in A) are highlighted with side-chains in blue for variations to FCoVIIs distant from the RBD, red for

236 variations close to the RBD, orange for the variation at aa546 similar to FIPV-2, and olive for the variation differing both from FCoVII

237 and pCCoV. A comparison showing a confidence model of the FCoV-23 RBD structure prediction paired with the CCoV-HuPN-2018-

238 canine aminopeptidase N (APN) is shown for orientation and binding visualization in the top right corner. Colors indicate confidence

239 with blue highlighting strong and red highlighting weak confidence.

Discussion

Recombination within the *Alphacoronavirus 1* species has been frequently observed previously and has even given rise to the FCoVII serotype[5,23,24](Figure 3B) in cats. Even complex recombination between FCoVI and CCoV has previously been observed[10]. However, in this work, we have identified a new subtype of FCoV that has recombined with a hypervirulent strain of pCCoV. The recombinant, which we propose naming FCoV-23, shows clearly distinct properties from previously observed FCoV infections. The sequence similarity found between FCoV-23 and CCoVII is higher than would be expected without an additional, recent recombination event.

Preliminary data suggest there may be no need for a biotype change to result in FIP and there is compelling evidence supportive of direct transmission of FCoV-23. However, more work is needed, including investigation into asymptomatic carriers. Of support, onset of FIP appears rapid and shows little discrimination in age of the infected cats. Most importantly, remarkably high sequence identity from isolates collected at different times and locations, is highly supportive of direct transmission of FCoV-23. The scale of this FIP outbreak has not been observed previously. Concerningly, Cyprus has a high population of unowned cats that are frequently relocated to other parts of Europe, and the wider world. The risk of spreading this outbreak is significant as evidenced by the first confirmed UK case[40]. This is exemplified by the recent confirmation of a first UK-imported case with further investigations into other cases ongoing.

CCoV infections in dogs are typically self-limiting, producing mild or asymptomatic enteritis. Previous work on the FCoV-23 close relative strain, CCoV NA/09 and CB/05, found the virus was hypervirulent and infected a range of organs in canine hosts. CCoV typically infects cells of the enteric tract, but pCCoVs were shown to spread to a range of internal organs, including intestine, lung, spleen, liver, kidney, lymph nodes, brain, and even T and B cells [34,41-43]. CB/05 has also been identified as responsible for small outbreaks[41].

The clinical signs of FCoV-23 are similar to those observed in classical FIP cases. However, FIP infection itself already shows a strong pantropism, affecting many organs in infected cats[25]. What is remarkable, is the high number of FCoV-23 positive cells observed in immunohistochemistry samples (Figure 1C). This is indicative of high viral loads, but must be validated through quantification. Furthermore, a relatively high percent (Supplementary Table 4) of confirmed cases in Cyprus was presented with neurological signs (28%), which is double of what would be expected with classical FIP (14%)[27]. This may be due to increased awareness of presentation or be inherent to FCoV-23 neurotropism; however, further investigation is required.

Significant changes to the spike protein in FCoV-23 may provide some clues as to the enhanced pathogenicity of this virus. FCoV-23, like other FCoVIIs and CCoVII, does not contain an FCS at the

275   S1/S2, and the related virus CCoV-HuPn-2018 was experimentally found to be uncleaved[39].
276   Uncleaved spike has been shown to be more stable than cleaved one and could enhance faecal
277   shedding and stability in the environment[44]. Conversely, the cleavage at S1/S2 may facilitate the
278   movement of the N-terminal domains and allow the RBD to adopt the receptor-binding-
279   competent form. However, the deletion of the N-terminal domain 0 may compensate for the
280   increased rigidity. Whilst a similar deletion between TGEV and PRCV was initially indicated as
281   the determinant between a primarily enteric and primarily respiratory tropism, respectively[45,46],
282   a recent study shows a different result *in vivo*[47]. Sialoside binding is an important feature of
283   coronavirus infections and may contribute to intracellular spread[48]. It is then all the more
284   surprising that FCoV-23 loses the sialoside-binding domain 0. However, whilst binding to
285   sialosides can enhance virus attachment and entry into host cells, binding to sugars can lead to
286   increased retention of virus on producer cells. Whilst some viruses, like influenza, solve this issue
287   by encoding their own sugar-cleaving enzyme, neuraminidase, coronaviruses must find a balance
288   through modifying glycoprotein binding[49]. Losing domain 0 could therefore be a trade-off to
289   enhance virus release. This may be compensated by the earlier discussed enhanced flexibility of
290   spike and increased binding efficiency at the RBD through mutation. These are manifold in the
291   FCoV-23 pCCoV recombinant and in particular mutations at position 546 (already possibly
292   associated with FIP) and 595 are likely to have a strong impact on aminopeptidase N receptor
293   binding (Figure 4C).

294   Recombination between FCoVI and pCCoVs is not surprising in that i) such recombinations have
295   been observed before, and ii) pCCoVs have evolved in Greece and south eastern Europe[34,42].
296   However, the emergence of pCCoV in Greece happened over 18 years ago, so the question as to
297   why this happened now is unclear yet. One possible explanation is the "right mutation, right time,
298   right place" theory. Recombination between feline and canine coronaviruses happen frequently
299   but as previous reports show, they rarely spread. Introduction of a more successful, spreading
300   variant to a dense population, like the cats in Cyprus, may be sufficient to allow this virus to cause
301   an outbreak. Whilst alphacoronaviruses show great cross-neutralizing activity[39], neutralising
302   immune evasion of FCoV-23 may be a contributing factor as indicated by the infection of cats of
303   all age groups. However, further investigation is required to determine shedding routes and
304   virulence. Preliminary RT-qPCR results and high virus-infected cell positivity in the colon are
305   strongly indicative of faecal shedding (data not shown and figure 1D). Analysis of historic
306   samples, (asymptomatic) cats and dogs may help further evaluate the origins of this virus.

307   This paper reports the emergence of a new *alphacoronavirus 1* feline/canine coronavirus that
308   shows high spreading potential with the associated pathology of lethal FIP if left untreated.
309   Further investigations into the properties of this new virus are now essential. Whilst antivirals,

310 including GS-441524 and molnupiravir were successfully used to treat some cats affected by

311 FCoV-23, early treatment is essential but associated costs are often prohibitive. Prevention of

312 spread and the development of new vaccines are important to stop this virus epizootic from

313 becoming a panzootic.

Acknowledgements

Author contributions

320 Conceptualization, C.A., A.W., D.G-M., S. M. and C.T-B.; Methodology, C.A., A.W., S.M., and C.T-B. ;
321 Validation, C.A., A.W., S.M. and C.T-B.; Formal Analysis, A.W., S.M. and C.T-B.; Investigation, C.A.,
322 A.W., D.E., M.O., S.F. , A.M., M.L., R.H., C.T-B.; Resources, C.A., A.W., D.E., M.L., A.H., A.Z., S.L., M.G. and
323 C.T-B.; Data Curation, A.W., S.M., and C. T-B.; Writing – Original Draft Preparation, C.A., A.W., and
324 C.T.B.; Writing – Review & Editing, C.A., A.W., S.F., D.G-M., S.M. and C.T-B.; Visualization, A.W., S.M.
325 and C.T-B.; Supervision, C.A. and C.T-B.; Project Administration, C.A. and C.T-B.; Funding
326 Acquisition, C.A., and C.T-B.

Funding

Competing interests

335 The authors declare no competing interests.

References

336 1   Olival, K. J. *et al.* Host and viral traits predict zoonotic spillover from mammals. *Nature* **546**,
338   646-650, doi:10.1038/nature22975 (2017).
339 2   Zhou, P. *et al.* Fatal swine acute diarrhoea syndrome caused by an HKU2-related coronavirus
340   of bat origin. *Nature* **556**, 255-258, doi:10.1038/s41586-018-0010-9 (2018).
341 3   Nova, N. Cross-Species Transmission of Coronaviruses in Humans and Domestic Mammals,
342   What Are the Ecological Mechanisms Driving Transmission, Spillover, and Disease Emergence?
343   *Front Public Health* **9**, 717941, doi:10.3389/fpubh.2021.717941 (2021).
344 4   Muller, N. F., Kistler, K. E. & Bedford, T. A Bayesian approach to infer recombination patterns
345   in coronaviruses. *Nat Commun* **13**, 4186, doi:10.1038/s41467-022-31749-8 (2022).
346 5   Herrewegh, A. A., Smeenk, I., Horzinek, M. C., Rottier, P. J. & de Groot, R. J. Feline coronavirus
347   type II strains 79-1683 and 79-1146 originate from a double recombination between feline
348   coronavirus type I and canine coronavirus. *Journal of virology* **72**, 4508-4514,
349   doi:10.1128/JVI.72.5.4508-4514.1998 (1998).
350 6   Boniotti, M. B. *et al.* Porcine Epidemic Diarrhea Virus and Discovery of a Recombinant Swine
351   Enteric Coronavirus, Italy. *Emerging infectious diseases* **22**, 83-87,
352   doi:10.3201/eid2201.150544 (2016).
353 7   Pedersen, N. C., Ward, J. & Mengeling, W. L. Antigenic relationship of the feline infectious
354   peritonitis virus to coronaviruses of other species. *Archives of virology* **58**, 45-53,
355   doi:10.1007/BF01315534 (1978).
356 8   Pedersen, N. C. A review of feline infectious peritonitis virus infection: 1963-2008. *Journal of*
357   *feline medicine and surgery* **11**, 225-258, doi:10.1016/j.jfms.2008.09.008 (2009).
358 9   Kannekens-Jager, M. M. *et al.* SARS-CoV-2 infection in dogs and cats is associated with contact
359   to COVID-19-positive household members. *Transbound Emerg Dis* **69**, 4034-4040,
360   doi:10.1111/tbed.14713 (2022).
361 10   Terada, Y. *et al.* Emergence of pathogenic coronaviruses in cats by homologous recombination
362   between feline and canine coronaviruses. *PLoS One* **9**, e106534,
363   doi:10.1371/journal.pone.0106534 (2014).
364 11   Attipa, C. *et al.* Concerning feline infectious peritonitis outbreak in Cyprus. *Vet Rec* **192**, 449-
365   450, doi:10.1002/vetr.3143 (2023).
366 12   Jaimes, J. A. & Whittaker, G. R. Feline coronavirus: Insights into viral pathogenesis based on
367   the spike protein structure and function. *Virology* **517**, 108-121,
368   doi:10.1016/j.virol.2017.12.027 (2018).
369 13   Amer, H. M. Bovine-like coronaviruses in domestic and wild ruminants. *Anim Health Res Rev*
370   **19**, 113-124, doi:10.1017/S1466252318000117 (2018).
371 14   Woo, P. C., Lau, S. K., Huang, Y. & Yuen, K. Y. Coronavirus diversity, phylogeny and interspecies
372   jumping. *Exp Biol Med (Maywood)* **234**, 1117-1127, doi:10.3181/0903-MR-94 (2009).
373 15   Small, J. D. & Woods, R. D. Relatedness of rabbit coronavirus to other coronaviruses. *Adv Exp*
374   *Med Biol* **218**, 521-527, doi:10.1007/978-1-4684-1280-2_68 (1987).
375 16   Gao, Y. Y. *et al.* An updated review of feline coronavirus: mind the two biotypes. *Virus Res* **326**,
376   199059, doi:10.1016/j.virusres.2023.199059 (2023).
377 17   Haake, C., Cook, S., Pusterla, N. & Murphy, B. Coronavirus Infections in Companion Animals:
378   Virology, Epidemiology, Clinical and Pathologic Features. *Viruses* **12**, doi:10.3390/v12091023
379   (2020).
380 18   Pedersen, N. C. An update on feline infectious peritonitis: virology and immunopathogenesis.
381   *Vet J* **201**, 123-132, doi:10.1016/j.tvjl.2014.04.017 (2014).
382 19   Vlasova, A. N. *et al.* Animal alphacoronaviruses found in human patients with acute respiratory
383   illness in different countries. *Emerg Microbes Infect* **11**, 699-702,
384   doi:10.1080/22221751.2022.2040341 (2022).
385 20   Saif, L. J. Animal coronaviruses: what can they teach us about the severe acute respiratory
386   syndrome? *Rev Sci Tech* **23**, 643-660, doi:10.20506/rst.23.2.1513 (2004).

387   21   Wang, Q., Vlasova, A. N., Kenney, S. P. & Saif, L. J. Emerging and re-emerging coronaviruses in
388   pigs. *Curr Opin Virol* **34**, 39-49, doi:10.1016/j.coviro.2018.12.001 (2019).
389   22   Corman, V. M., Muth, D., Niemeyer, D. & Drosten, C. Hosts and Sources of Endemic Human
390   Coronaviruses. *Adv Virus Res* **100**, 163-188, doi:10.1016/bs.aivir.2018.01.001 (2018).
391   23   Jaimes, J. A., Millet, J. K., Stout, A. E., Andre, N. M. & Whittaker, G. R. A Tale of Two Viruses:
392   The Distinct Spike Glycoproteins of Feline Coronaviruses. *Viruses* **12**, doi:10.3390/v12010083
393   (2020).
394   24   Le Poder, S. Feline and canine coronaviruses: common genetic and pathobiological features.
395   *Advances in virology* **2011**, 609465, doi:10.1155/2011/609465 (2011).
396   25   Tasker, S. *et al.* Feline Infectious Peritonitis: European Advisory Board on Cat Diseases
397   Guidelines. *Viruses* **15**, doi:10.3390/v15091847 (2023).
398   26   Zehr, J. D. *et al.* Natural selection differences detected in key protein domains between non-
399   pathogenic and pathogenic feline coronavirus phenotypes. *Virus Evol* **9**, vead019,
400   doi:10.1093/ve/vead019 (2023).
401   27   Taylor, S. S. *et al.* Retrospective study and outcome of 307 cats with feline infectious
402   peritonitis treated with legally sourced veterinary compounded preparations of remdesivir
403   and GS-441524 (2020-2022). *Journal of feline medicine and surgery* **25**, 1098612X231194460,
404   doi:10.1177/1098612X231194460 (2023).
405   28   Descoteaux, J. P. *et al.* An enteric coronavirus of the rabbit: detection by immunoelectron
406   microscopy and identification of structural polypeptides. *Archives of virology* **84**, 241-250,
407   doi:10.1007/BF01378976 (1985).
408   29   Lefkowitz, E. J. *et al.* Virus taxonomy: the database of the International Committee on
409   Taxonomy of Viruses (ICTV). *Nucleic Acids Res* **46**, D708-D717, doi:10.1093/nar/gkx932 (2018).
410   30   Whittaker, G. R., Andre, N. M. & Millet, J. K. Improving Virus Taxonomy by Recontextualizing
411   Sequence-Based Classification with Biologically Relevant Data: the Case of the
412   Alphacoronavirus 1 Species. *mSphere* **3**, doi:10.1128/mSphereDirect.00463-17 (2018).
413   31   Wang, Y. T., Su, B. L., Hsieh, L. E. & Chueh, L. L. An outbreak of feline infectious peritonitis in a
414   Taiwanese shelter: epidemiologic and molecular evidence for horizontal transmission of a
415   novel type II feline coronavirus. *Vet Res* **44**, 57, doi:10.1186/1297-9716-44-57 (2013).
416   32   Chang, H. W., de Groot, R. J., Egberink, H. F. & Rottier, P. J. Feline infectious peritonitis: insights
417   into feline coronavirus pathobiogenesis and epidemiology based on genetic analysis of the
418   viral 3c gene. *J Gen Virol* **91**, 415-420, doi:10.1099/vir.0.016485-0 (2010).
419   33   Decaro, N. *et al.* Recombinant canine coronaviruses related to transmissible gastroenteritis
420   virus of Swine are circulating in dogs. *Journal of virology* **83**, 1532-1537,
421   doi:10.1128/JVI.01937-08 (2009).
422   34   Ntafis, V. *et al.* Molecular characterization of a canine coronavirus NA/09 strain detected in a
423   dog's organs. *Archives of virology* **157**, 171-175, doi:10.1007/s00705-011-1141-6 (2012).
424   35   Martin, D. P., Posada, D., Crandall, K. A. & Williamson, C. A modified bootscan algorithm for
425   automated identification of recombinant sequences and recombination breakpoints. *AIDS Res*
426   *Hum Retroviruses* **21**, 98-102, doi:10.1089/aid.2005.21.98 (2005).
427   36   Martin, D. P. *et al.* RDP5: a computer program for analyzing recombination in, and removing
428   signals of recombination from, nucleotide sequence datasets. *Virus Evolution* **7**,
429   doi:10.1093/ve/veaa087 (2020).
430   37   Smith, J. M. Analyzing the mosaic structure of genes. *J Mol Evol* **34**, 126-129,
431   doi:10.1007/bf00182389 (1992).
432   38   Schultze, B. *et al.* Transmissible gastroenteritis coronavirus, but not the related porcine
433   respiratory coronavirus, has a sialic acid (N-glycolylneuraminic acid) binding activity. *Journal*
434   *of virology* **70**, 5634-5637, doi:10.1128/JVI.70.8.5634-5637.1996 (1996).
435   39   Tortorici, M. A. *et al.* Structure, receptor recognition, and antigenicity of the human
436   coronavirus CCoV-HuPn-2018 spike glycoprotein. *Cell* **185**, 2279-2291 e2217,
437   doi:10.1016/j.cell.2022.05.019 (2022).

16

| 438 439 | 40 | Maggi, R. G. *et al.* Vector-borne and other pathogens of potential relevance disseminated by relocated cats. *Parasit Vectors* **15**, 415, doi:10.1186/s13071-022-05553-8 (2022). |

40   Maggi, R. G. *et al.* Vector-borne and other pathogens of potential relevance disseminated by relocated cats. *Parasit Vectors* **15**, 415, doi:10.1186/s13071-022-05553-8 (2022).

41   Buonavoglia, C. *et al.* Canine coronavirus highly pathogenic for dogs. *Emerging infectious diseases* **12**, 492-494, doi:10.3201/eid1203.050839 (2006).

42   Decaro, N. *et al.* Molecular characterisation of the virulent canine coronavirus CB/05 strain. *Virus Res* **125**, 54-60, doi:10.1016/j.virusres.2006.12.006 (2007).

43   Marinaro, M. *et al.* Prolonged depletion of circulating CD4+ T lymphocytes and acute monocytosis after pantropic canine coronavirus infection in dogs. *Virus Res* **152**, 73-78, doi:10.1016/j.virusres.2010.06.006 (2010).

44   Wrobel, A. G. *et al.* SARS-CoV-2 and bat RaTG13 spike glycoprotein structures inform on virus evolution and furin-cleavage effects. *Nat Struct Mol Biol* **27**, 763-767, doi:10.1038/s41594-020-0468-7 (2020).

45   Sanchez, C. M. *et al.* Targeted recombination demonstrates that the spike gene of transmissible gastroenteritis coronavirus is a determinant of its enteric tropism and virulence. *Journal of virology* **73**, 7607-7618, doi:10.1128/JVI.73.9.7607-7618.1999 (1999).

46   Sanchez, C. M., Pascual-Iglesias, A., Sola, I., Zuniga, S. & Enjuanes, L. Minimum Determinants of Transmissible Gastroenteritis Virus Enteric Tropism Are Located in the N-Terminus of Spike Protein. *Pathogens* **9**, doi:10.3390/pathogens9010002 (2019).

47   Wang, G. *et al.* The N-Terminal Domain of Spike Protein Is Not the Enteric Tropism Determinant for Transmissible Gastroenteritis Virus in Piglets. *Viruses* **11**, doi:10.3390/v11040313 (2019).

48   Qing, E., Hantak, M., Perlman, S. & Gallagher, T. Distinct Roles for Sialoside and Protein Receptors in Coronavirus Infection. *mBio* **11**, doi:10.1128/mBio.02764-19 (2020).

49   Buchanan, C. J. *et al.* Pathogen-sugar interactions revealed by universal saturation transfer analysis. *Science* **377**, eabm3125, doi:10.1126/science.abm3125 (2022).

50   Gut, M., Leutenegger, C. M., Huder, J. B., Pedersen, N. C. & Lutz, H. One-tube fluorogenic reverse transcription-polymerase chain reaction for the quantitation of feline coronaviruses. *J Virol Methods* **77**, 37-46, doi:10.1016/s0166-0934(98)00129-3 (1999).

51   Quick, J. *et al.* Multiplex PCR method for MinION and Illumina sequencing of Zika and other virus genomes directly from clinical samples. *Nature Protocols* **12**, 1261-1276, doi:10.1038/nprot.2017.066 (2017).

52   Sayers, E. W. *et al.* Database resources of the national center for biotechnology information. *Nucleic Acids Res* **50**, D20-d26, doi:10.1093/nar/gkab1112 (2022).

53   Vierstraete, A. R. & Braeckman, B. P. Amplicon_sorter: A tool for reference-free amplicon sorting based on sequence similarity and for building consensus sequences. *Ecol Evol* **12**, e8603, doi:10.1002/ece3.8603 (2022).

54   Li, H. Minimap2: pairwise alignment for nucleotide sequences. *Bioinformatics* **34**, 3094-3100, doi:10.1093/bioinformatics/bty191 (2018).

55   Altschul, S. F., Gish, W., Miller, W., Myers, E. W. & Lipman, D. J. Basic local alignment search tool. *J Mol Biol* **215**, 403-410, doi:10.1016/s0022-2836(05)80360-2 (1990).

56   Robinson, J. T. *et al.* Integrative genomics viewer. *Nature Biotechnology* **29**, 24-26, doi:10.1038/nbt.1754 (2011).

57   Amanda, W. *et al.* No part gets left behind: Tiled nanopore sequencing of whole ASFV genomes stitched together using Lilo. *bioRxiv*, 2021.2012.2001.470769, doi:10.1101/2021.12.01.470769 (2021).

58   Katoh, K., Misawa, K., Kuma, K. i. & Miyata, T. MAFFT: a novel method for rapid multiple sequence alignment based on fast Fourier transform. *Nucleic Acids Research* **30**, 3059-3066, doi:10.1093/nar/gkf436 (2002).

59   Kumar, S., Stecher, G. & Tamura, K. MEGA7: Molecular Evolutionary Genetics Analysis Version 7.0 for Bigger Datasets. *Mol Biol Evol* **33**, 1870-1874, doi:10.1093/molbev/msw054 (2016).

488 60   Nguyen, L. T., Schmidt, H. A., von Haeseler, A. & Minh, B. Q. IQ-TREE: a fast and effective
489   stochastic algorithm for estimating maximum-likelihood phylogenies. *Mol Biol Evol* **32**, 268-
490   274, doi:10.1093/molbev/msu300 (2015).
491 61   Rambaut, A., Lam, T. T., Max Carvalho, L. & Pybus, O. G. Exploring the temporal structure of
492   heterochronous sequences using TempEst (formerly Path-O-Gen). *Virus Evolution* **2**,
493   doi:10.1093/ve/vew007 (2016).
494 62   Letunic, I. & Bork, P. Interactive Tree Of Life (iTOL) v5: an online tool for phylogenetic tree
495   display and annotation. *Nucleic Acids Research* **49**, W293-W296, doi:10.1093/nar/gkab301
496   (2021).
497 63   Silva, G. G. Z. *et al.* Combining de novo and reference-guided assembly with scaffold_builder.
498   *Source Code for Biology and Medicine* **8**, 23, doi:10.1186/1751-0473-8-23 (2013).
499 64   Thompson, J. D., Higgins, D. G. & Gibson, T. J. CLUSTAL W: improving the sensitivity of
500   progressive multiple sequence alignment through sequence weighting, position-specific gap
501   penalties and weight matrix choice. *Nucleic Acids Res* **22**, 4673-4680,
502   doi:10.1093/nar/22.22.4673 (1994).
503 65   Waterhouse, A. *et al.* SWISS-MODEL: homology modelling of protein structures and
504   complexes. *Nucleic Acids Res* **46**, W296-W303, doi:10.1093/nar/gky427 (2018).
505

Methods

Enrolment of FIP cases in Cyprus

The electronic records of Vet Dia Gnosis in Limassol, Cyprus were searched for any positive FCoV RT-PCR cases from September 2021 up to August 2023. The cases to be enrolled needed to have compatible clinicopathological findings for FIP as recently outlined by the European Advisory Board on Cat Diseases Guidelines[25] as well having a positive RT-PCR for FCoV in one of the following samples: peritoneal fluid, pleural fluid, cerebrospinal fluid and granuloma fine needle aspiration biopsies or tissue biopsies. The original samples were submitted to the Vet Dia Gnosis commercial laboratory (Limassol, Cyprus) by local veterinarians and then submitted to LABOKLIN commercial laboratory (Bad Kissingen, Germany). Ethical approval for this study was granted by the Pancyprian Vet Association. According to the terms and conditions of the Vet Dia Gnosis, as well as the Cypriot legislation [The Dogs LAW, N. 184 (I)/2002], no special permission from animal owners or the animal welfare commission is needed for additional testing on residual sample material once diagnostics are completed. According to the terms and conditions of the LABOKLIN laboratory, as well as the RUF-55.2.2.2532-1-86-5 decision of the government of Lower Franconia, no special permission from animal owners or the animal welfare commission is needed for additional testing on residual sample material once diagnostics are completed.

Sample from cat imported to the UK

Two UK veterinary practices contacted the Royal Dick School of Veterinary Sciences (R(D)SVS) with suspected cases of FIP in cats recently imported from Cyprus. Peritoneal fluid samples were taken from the cats and sent to R(D)SVS for further testing and for sequencing at The Roslin Institute with the consent of the cats' owners. The veterinary practices and the cats' owners were kept informed at all stages.

Histopathology and immunohistochemistry

A sub-set of cases (n=4) from the FIP cats diagnosed after January 2023 with available tissue specimens were selected. Tissue specimens were carefully obtained and immediately fixed in 10% buffered formalin. Following fixation, the tissues were processed by embedding, 4μm sectioning, and subsequent staining with hematoxylin and eosin (H&E). The inclusion criteria were defined based on comprehensive histopathological assessments. Specifically, emphasis was placed on identifying the characteristic FIP-associated histological hallmarks, which encompassed vasculitis, phlebitis, and periphlebitis. Consecutive tissue sections were mounted onto charged slides. Following pre-treatment for 5 min at 110°C in 0.01M pH 6 citrate buffer, slides were incubated for 30 min at room temperature with primary mouse monoclonal anti-feline coronavirus antibody at 1:400 (BioRad, MCA 2194). The EnVision anti-mouse system was used for visualization according to the manufacturer's instructions (Agilent).

19

RNA extraction and cDNA synthesis

RNA from specimens from Cyprus underwent automated total nucleic acid extraction using the MagNA Pure 96 DNA AND Viral NA Small Volume kit (Roche Diagnostics). RT-PCR for FCoV was performed at Laboklin Bad Kissingen, Germany[50].

RNA samples from cats imported to the UK from Cyprus were extracted using the QIAamp viral RNA extraction kit (Qiagen) according to the manufacturer's instructions.

cDNA synthesis on all RNA samples was carried out using LunaScript RT SuperMix Kit (NEB) with 16 μl template RNA in 20 μl reactions according to the manufacturer's instructions.

Primer design and PCR amplification

A set of primers for 1kb tiled amplification were designed initially using primalscheme[51] with available FCoV genomes on NCBI[52], and then by manual redesigns. Currently there is not a working scheme for the entire genome, however, through multiple redesigns on multiple samples it was possible to amplify sections which, when combined, cover the entire genome with one gap. It should be noted that sequences obtained from this process do not all originate from the same sample, and the genome assembled from these is representative at a population level rather than an individual level, and therefore may not accurately represent virus present within an individual. Efforts are ongoing to create a working tiled amplification scheme. The primer sequences used here are in Supplementary Table 18. The PCRs for these multiplexed amplifications used the same conditions described below, but with multiplexed primers.

DNA was amplified using primers targeting the majority of the spike region and incorporating a flanking region of known FCoV sequence, with an expected amplicon size of around 3.7 kb. These were designed based on previously amplified flanking sequences during the tiled amplification design process: forward primer 5'-GACGCAGACTTCAGTGTTA-3'; and reverse primer 5'-ACCATTATGCCATTRTARTA-3'. These primers do also produce offtarget amplification of the feline growth hormone receptor. Additional amplicons designed during the tiled amplicon designing process were used to amplify regions of POL1ab and Orf3c/E/M from the samples (Supplementary Table 18).

PCR amplification was carried out on each sample using VeriFi Hot Start Mix (PCR Biosystems), 1.25μl 10μM forward and reverse primers and 2μl cDNA in a 25μl reaction. Amplification was performed with the following PCR conditions: initial denaturation at 95°C for 1 minute, then 35 cycles of denaturation at 95°C for 15 seconds, annealing at 52°C for 15 seconds, extension at 72°C for 4 minutes, followed by a final extension at 72°C for 5 minutes. Amplified DNA was purified using AMPure XP beads (Beckman Coulter). The amplicons targeting POL1ab and NSP3c/E/M

20

574 were amplified in a pool with other primer pairs using the same PCR conditions but with 4μl cDNA

575 in the reaction instead of 2μl.

576 **Nanopore sequencing**

577 Amplicons were quantified using Qubit (Thermo Fisher) High Sensitivity assays and diluted to

578 150ng DNA per sample in 12μl nuclease-free water. Libraries were prepared using Oxford

579 Nanopore Technologies' (ONT) NBD112.96 ligation kit following the manufacturer's protocol for

580 amplicon sequencing with some modifications. Due to unavailability of NBD112.96 kit reagent

581 AMII H, following ligation of barcodes a second end-prep was carried out using the Ultra II End

582 Repair module (NEB). The rest of the protocol was carried out from the adapter ligation stage as

583 per manufacturer's protocol for LSK112 using the AMX-F adapter supplied in the early access

584 Q20+ version of kit 112. The library was loaded onto a MinION R10.4 flow cell and sequencing

585 was carried out on a GridION sequencing device.

586 In order to identify the virus present in one of the UK cases as quickly as possible, only the spike

587 amplicon was amplified and the sample sequenced using ONT RAD004 rapid sequencing kit on

588 an R9.4 flow cell following manufacturer's protocol. The other UK case was amplified at an earlier

589 time and was included in a sequencing run with the Cypriot samples, the data from that sample

590 was treated in the same way as the Cypriot samples and was the sample later found to have the

591 non-recombinant FCoVI spike.

592 **Bioinformatic analysis**

593 Basecalling and demultiplexing was carried out on the GridION sequencing device (ONT) using

594 Guppy (v2.24-r1122) on super accurate mode, specifying --require_barcodes_both_ends and

595 using appropriate super accurate basecalling models for each of the different sequencing

596 methods used. Following basecalling, amplicon_sorter[53] (v2023-06-19) was used to identify

597 consensus amplicons between 3kb and 5kb without using a reference. Spike amplicons were

598 identified from the output via alignment with minimap2[54] (v2.22) to the spike from the first

599 sample we sequenced (Cypriot_G7_Gi_6739) for which a consensus was made using the same

600 process, with the correct amplicon identified via BLAST[55]. The identified amplicons were polished

601 with medaka (v1.8.0, ONT). For the UK case which was sequenced with the rapid kit, because the

602 reads were fragmented by the library prep process, reads were used to polish the

603 Cypriot_G7_Gi_6739 sequence using medaka. The reads were aligned to the polished sequence

604 with minimap2 and visualized with IGV[56] (v2.11.1) to visually confirm the reads supported the

605 consensus sequence and that it had not been biased by the reference used. The amplicons in

606 POL1ab and Orf3c/E/M were assembled and polished using LILO[57]. Multisequence alignments

607 were carried out for each of the regions using mafft[58] (v7.49) against all complete genomes of

608 CCoV and FCoV genomes available on NCBI using the --adjustdirection flag. Alignments were

609   visualized in Mega7[59] and sequences with poor sequencing quality were removed. All
610   downloaded genomes were trimmed down to each of the target regions amplified from our
611   samples. Maximum likelihood trees were constructed using IQ-TREE[60] (v2.0.5). TempEst[61]
612   (v1.5.3) was used to determine the best fitting root for the trees, and visualizations and
613   annotations of the trees were done using iTOL[62] (v6.8.1). The trees were combined into figures
614   using BioRender.

615   To assemble a representative genome for the population, all of the samples for which we had
616   sequencing data were run through LILO. The polished amplicons were mapped to a single fasta
617   file containing an FCoVI (MT239440.1) and a CCoVII (KP981644.1) using minimap2 and
618   visualized with IGV, with only the amplicons from the spike region aligning to CCoVII.
619   Representative amplicons covering the entire genome were selected and scaffolded using
620   scaffold_builder[63] with MT239440.1 as a reference. The raw reads were trimmed by 50bp to
621   remove adapters and barcodes and they were used to polish this scaffold using medaka. Mafft
622   was used to align this genome to representative genomes from *Alphacoronavirus 1* with Canine
623   Respiratory Coronavirus as an outgroup, and Mega7 was used to create a neighbour join tree
624   which was visualized and annotated with iTOL. BLAST was used to align reads that span the gap
625   to existing CCoV and FCoV genomes to determine the likely breakpoint (results in Supplementary
626   Figure 6).

627   A multisequence alignment between the genome and MT239440.1, LC742526.1 and KP981644.1
628   was carried out using ClustalW[64] in Mega7, and recombination analysis carried out using RDP5[36]
629   (v.5.45) on default settings.

630   **Structure prediction of spike deletion variants**
631   SWISS-MODEL structure prediction and analysis (https://swissmodel.expasy.org/, accessed
632   October 2023)[65] were used to model the partial, high confidence N-terminal sequence of a
633   full-length spike (1008aa) and a deletion spike (797aa). To model the G8 Cypriot full-length spike,
634   we used the alphacoronavirus 1 experimentally resolved CCoV-HuPn-2018[39] structure as a
635   template. Modelling against the 7usa.1.a, swung out confirmation, yielded GMQE 0.60 and Global
636   QMEAND of 0.68±0.05 with a sequence identity of 88.97% and against 7us6.1.A, proximal
637   confirmation, yielded GMQE of 0.62 and Global QMEAND of 0.58±0.05 with a sequence identity of
638   81.03%. Modelling of C10 spike, C-terminal deletion, against 7usa.1.A, swung out confirmation,
639   yielded GMQE 0.74 and Global QMEAND of 0.69±0.05 with a sequence identity of 88.66% and
640   against 7us6.1.A, proximal confirmation of HuPN, yielded GMQE of 0.76 and Global QMEAND of
641   0.70±0.05 with a sequence identity of 88.42%.

642 The receptor binding domain was modelled using the 7u0I.1B structure, again CCoV-HuPn-
643 2018[39] complexed with canine APN as a template. GMQE was 0.89 and Global QMEAND 0.85±0.07
644 with a sequence identity of 92.41%. PDB files are available in the supplementary materials.